HYDROLOGICAL PROCESSES
Hydrol. Process. **21**, 35–50 (2007)
Published online 16 May 2006 in Wiley InterScience
(www.interscience.wiley.com) DOI: 10.1002/hyp.6175

Runoff and suspended sediment yields from an unpaved road segment, St John, US Virgin Islands

Carlos E. Ramos-Scharrón[1]* and Lee H. MacDonald[2]

[1] *Department of Geosciences, Colorado State University, Fort Collins, CO 80523-1482, USA*
[2] *Department of Forest, Rangeland, and Watershed Stewardship, Colorado State University, Fort Collins, CO 80523-1472, USA*

Abstract:

Unpaved roads are believed to be the primary source of terrigenous sediments being delivered to marine ecosystems around the island of St John in the eastern Caribbean. The objectives of this study were to: (1) measure runoff and suspended sediment yields from a road segment; (2) develop and test two event-based runoff and sediment prediction models; and (3) compare the predicted sediment yields against measured values from an empirical road erosion model and from a sediment trap. The runoff models use the Green–Ampt infiltration equation to predict excess precipitation and then use either an empirically derived unit hydrograph or a kinematic wave to generate runoff hydrographs.

Precipitation, runoff, and suspended sediment data were collected from a 230 m long, mostly unpaved road segment over an 8-month period. Only 3–5 mm of rainfall was sufficient to initiate runoff from the road surface. Both models simulated similar hydrographs. Model performance was poor for storms with less than 1 cm of rainfall, but improved for larger events. The largest source of error was the inability to predict initial infiltration rates.

The two runoff models were coupled with empirical sediment rating curves, and the predicted sediment yields were approximately 0·11 kg per square meter of road surface per centimetre of precipitation. The sediment trap data indicated a road erosion rate of 0·27 kg m^{-2} cm^{-1}. The difference in sediment production between these two methods can be attributed to the fact that the suspended sediment samples were predominantly sand and silt, whereas the sediment trap yielded mostly sand and gravel. The combination of these data sets yields a road surface erosion rate of 0·31 kg m^{-2} cm^{-1}, or approximately 36 kg m^{-2} $year^{-1}$. This is four orders of magnitude higher than the measured erosion rate from undisturbed hillslopes. The results confirm the importance of unpaved roads in altering runoff and erosion rates in a tropical setting, provide insights into the controlling processes, and provide guidance for predicting runoff and sediment yields at the road-segment scale. Copyright © 2006 John Wiley & Sons, Ltd.

KEY WORDS road erosion; runoff modelling; kinematic wave; unit hydrograph; eastern Caribbean

Received 20 August 2004; Accepted 28 July 2005

INTRODUCTION

Problem statement

Roads alter the processes that control the storage and distribution of water on the landscape. The most obvious effect of roads is to increase the frequency and magnitude of surface runoff by creating a compacted, low-permeability surface (Bren and Leitch, 1985; Harden, 1992; Ziegler and Giambelluca, 1997). Roads also affect runoff by intercepting subsurface flows (e.g. Megahan, 1972) and disrupting natural drainage patterns (Montgomery, 1994; Borga *et al*., 2004; Dutton *et al*., 2005). Unpaved roads have an equally large or greater effect on the rate at which sediment is produced, routed, and eventually exported from a catchment. Surface erosion rates from unpaved roads are typically many times higher than the erosion rate from undisturbed hillslopes (e.g. Megahan, 1978; Reid, 1981; Megahan *et al*., 2001; Ramos-Scharrón, 2004). Hillslope gullies formed by the concentration of road drainage are another source of sediment and an important conduit for delivering runoff and sediment to the fluvial network (Wemple *et al*., 1996; Croke and Mockler, 2001; Croke *et al*., 2005). Roads also have been shown to increase the frequency of mass-wasting events (e.g. Gresswell *et al*., 1979; Wemple *et al*., 2001) and watershed-scale sediment yields (e.g. Rice *et al*., 1979; Anderson and Potts, 1987).

A three-decade long decline in coral reef cover over the Caribbean region has been associated with localized anthropogenic stresses, including excess delivery of land-based sediments (Gardner *et al*., 2003). A high concentration of sediment in the water column reduces the amount of light available for photosynthesis by symbiotic algae, and the settling of sediment can smother existing coral or reduce the surface area suitable for new coral growth (Hubbard, 1987). On the island of St John, the observed declines in live coral reef cover over the past 20 years may be due to sedimentation from coastal development (Rogers, 1998). Sedimentation and the decline in coral reefs is a critical issue in many tropical areas because of the importance of coral reefs for tourism and sustaining local communities.

Earlier studies have shown that unpaved roads on St John can increase sediment production rates at the

* Correspondence to: Carlos E. Ramos-Scharrón, Department of Geography and the Environment, University of Texas at Austin, 1 University Station, A3100 Austin, TX 78712-1098, USA. E-mail: cramos@irf.org

plot and hillslope scale by several orders of magnitude relative to undisturbed areas (MacDonald *et al*., 2001), and that unpaved roads are probably the primary source of fine sediment being delivered to the marine environment (MacDonald *et al*., 1997; Anderson and MacDonald, 1998; Ramos-Scharrón and MacDonald, 2003). A key limitation of earlier studies is that runoff rates were not measured and sediment yields were aggregated values from one or more storms. Another problem is that the sediment traps used to measure sediment production generally underestimate the amount of silts and clays being eroded from the road surface (Sampson, 1999), and these smaller particles may pose the greatest threat to the coral reefs. More detailed measurements and a process-based understanding are needed to predict runoff and sediment yields more accurately at the road segment scale. More physically based models may be better able to predict runoff and erosion rates from extreme events and be useful for a wider range of conditions.

The main objectives of this study were to: (1) measure runoff and suspended sediment production from a mostly unpaved road segment during natural rainfall events; (2) use these data to calibrate and test two runoff models; (3) couple the runoff models with sediment rating curves to predict sediment yields; and (4) compare the predicted sediment yields against predicted sediment yields from a locally calibrated, empirical road erosion model and sediment trap data (Ramos-Scharrón and MacDonald, 2005). The results provide insights into the processes controlling road runoff and erosion, and can help improve the road erosion component in a new, geographic information system-based sediment budget model (Ramos-Scharrón, 2004; Ramos-Scharrón and MacDonald, in press).

Event-based models for predicting road surface runoff and sediment yields generally share a three-step structure. First, the models calculate the rainfall excess for each time step by subtracting the estimated infiltration from rainfall intensity. Infiltration can be predicted by applying an average infiltration rate to all events (e.g. Reid, 1981) or by using a time-dependent infiltration capacity curve (e.g. Luce, 1990; Ziegler *et al*., 2001a). The second step is to transform the excess precipitation into an outflow hydrograph using empirical unit hydrographs (UHs; e.g. Reid and Dunne, 1984; Kahklen, 1994) or a kinematic wave approach (e.g. Simons *et al*., 1977, 1978; Luce and Cundy, 1992). The third step is to use the predicted runoff to calculate sediment production rates from empirical sediment rating curves (e.g. Reid and Dunne, 1984) or more physically based erosion and sediment transport models (e.g. Simons *et al*., 1977, 1978).

This study developed, calibrated, and tested the performance of two runoff models. The first model (GA-UH) calculated infiltration rates using the Green–Ampt (GA) equation. The precipitation excess estimated by this model was transformed into outflow using an empirically derived UH. The second model (GA-KW) also used the GA equation, but combined it with a kinematic wave (KW) routing approach. Both models were coupled with empirical sediment rating curves to estimate sediment yields.

Study area

St John lies in the eastern Caribbean approximately 80 km east of Puerto Rico. At 50 km^2, it is the third largest island of the US Virgin Islands. Over half of the island and 70 km^2 of the surrounding waters are protected as a national park or monument. The topography of St John is very rugged, as more than 80% of the island has slopes greater than 30% (Anderson, 1994). Vegetation is dominated by dry evergreen forests, shrublands, and moist tropical forests (Woodbury and Weaver, 1987).

The climate of St John is characterized as dry tropical. Erosion is an important concern because mean precipitation usually exceeds 100 cm $year^{-1}$ and precipitation intensities are relatively high. Five different precipitation zones have been identified on St John, and annual rainfall in the different zones ranges from 89–102 cm $year^{-1}$ in the lowest zone on the eastern end of the island to 127–140 cm $year^{-1}$ at higher elevations (Bowden *et al*., 1970). Hurricanes and other low-pressure systems generate a large proportion of the rainfall between May and November, whereas cold fronts control the rainfall regime during the rest of the year (Calversbert, 1970). At Caneel Bay, which lies in the middle precipitation zone, the 15 min rainfall intensity exceeds 10 cm h^{-1} at least once a year, and these high rainfall intensities are generally embedded within the largest storms. The annual erosivity at Caneel Bay is estimated to be 13 500 MJ mm ha^{-1} h^{-1} (Sampson, 1999).

Rapid development on privately owned lands has led to a dense network of unpaved roads. Typical roads are 4–5 m wide with slopes ranging up to 22% (Ramos-Scharrón, 2004). The construction and maintenance standards of public roads and private driveways are generally very poor. The steep gradients, poor drainage design, and high rainfall erosivity result in the development of deep rills on the road surfaces. Even though nearly all of the traffic consists of light vehicles, the steeper, more frequently travelled roads may have to be regraded once or twice a year. The major arterial roads are paved, but the high cost means that other roads typically are paved only for relatively short road segments as a spontaneous response to homeowner frustrations in trying to navigate severely rilled roads. The lack of proper design and site preparation means that effective road drainage structures (i.e. ditches, culverts, and cross-drains) are generally lacking, and both the paved and unpaved portions deteriorate rapidly.

Rainfall, runoff, and suspended sediment concentrations were measured for a 230 m long road segment in the Maho Bay area on the north-central portion of St John (Figures 1 and 2a). The study segment (hereafter referred as Maho-Road) was chosen because it was quickly accessible during most storm events and its drainage pattern

DOI: 10.1002/hyp

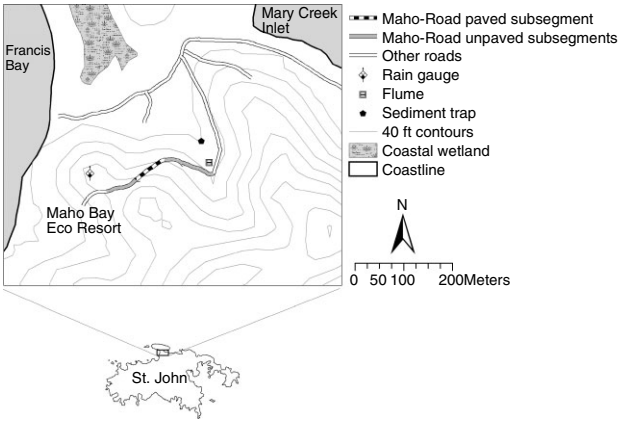

Figure 1. Map of the Maho Bay area showing the road segment that was studied and the location of the rain gauge, cutthroat flume, and sediment trap

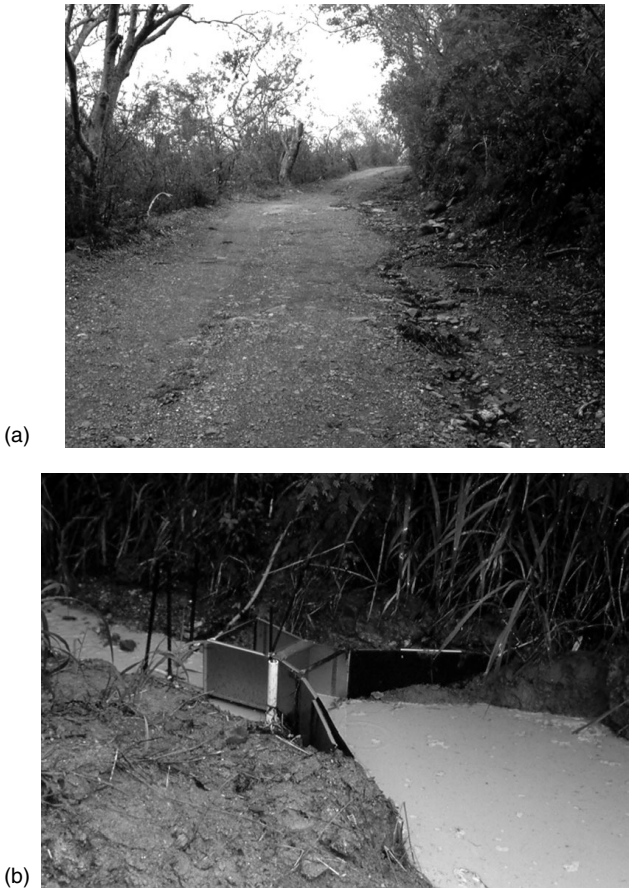

Figure 2. Pictures of (a) the two lower sections of Maho-Road and (b) a portable cutthroat flume similar to the one used to measure runoff from Maho-Road

allowed the installation of both runoff measuring equipment and a sediment trap. In addition, the drainage area of the road surface could be clearly delineated and was relatively constant from storm to storm. The mean slope of Maho-Road is 12·5%, and its length, slope, and width are representative of many other road segments on St John (Ramos-Scharrón, 2004).

Maho-Road was divided into four subsegments according to variations in road surface material and slope (Table I). The second subsegment from the top is much steeper so it had been paved with a thin layer of non-reinforced concrete placed on top of a poorly prepared native surface. Some of the concrete has broken apart to expose the underlying native soil, and this partially paved section accounts for about 15% of the total road segment area. The unpaved portions of Maho-Road are regraded once or twice a year to facilitate the daily traffic flow of four to six heavy trucks and 100–270 light vehicles into the Maho Bay Eco Resort (Figure 1).

Table I. Characteristics of the four subsegments comprising Maho-Road

Subsegment	Length (m)	Mean width (m)	Mean slope (m m^{-1})	Comments
1	49	4·4	0·10	Top section, unpaved
2	48	4·0	0·26	Partially-paved
3	40	6·0	0·13	Unpaved
4	95	6·3	0·09	Lowermost section, unpaved
Total or mean	232	5·4	0·12	

The lithology in the Maho Bay area consists of metamorphosed volcanic wacke, conglomerates, siltstones, limestones, and some basalt (Rankin, 2002). The soils are gravelly loams that are approximately 30 cm thick, moderately permeable, well drained, and underlain by nearly impervious material (NRCS, 1998). These soil characteristics, when combined with a dense vegetative cover and abundant macropores, are largely responsible for the lack of precipitation-excess overland flow on undisturbed surfaces (MacDonald *et al*., 2001). Mean annual rainfall in this area is 114–127 cm (Bowden *et al*., 1970).

METHODS

Field methods

The 5 min precipitation intensities were measured by a tipping-bucket rain-gauge located about 50 m from the top end of Maho-Road (Figure 1). This gauge had a resolution of 0·25 mm and data were collected from 2 September 1999 to 16 May 2000. Individual storms were defined as a precipitation event separated from other events by at least 1 h with no precipitation index. A time-weighted antecedent precipitation was calculated for each storm (Dunne and Leopold, 1978). The index for each successive day with no rainfall is simply multiplied by $0{\cdot}9^k$, where k equals the number of subsequent days without rainfall. The index for any given storm equals the index at the beginning of the day plus any additional rainfall that fell on that day prior to the storm of interest.

A 20·3 cm portable cutthroat flume was used to measure runoff (Figure 2b). The flume was installed in a natural swale about 10 m downslope from a broad dip that diverted all of the runoff from Maho-Road (Figure 1). The flume had a maximum capacity of 65

DOI: 10.1002/hyp

l s^{-1}, and this converts to a runoff rate of 19 cm h^{-1} for the 1246 m^2 area of Maho-Road. Stage was measured by a pressure transducer in a stilling well attached to the flume, and these data were collected at 5 min intervals. An equation provided by the flume manufacturer (Baski, Inc.) was used to convert the stage data to discharge. During some runoff events, manual staff gauge readings were taken at 2·5 min intervals to check the accuracy and improve the time resolution of the automated data.

Automated data collection was interrupted several times during the study period. From 13 to 23 October 1999 the orifice leading to the stilling well was clogged with sediment, so reliable data were available only for the three storm events with manual staff gauge readings. The flume was dislodged by high flows on 25 October 1999 and it was not reset until 30 October 1999. The flume also was dislodged on 17 November 1999 by runoff from Hurricane Lenny, and measurements did not resume until 17 December 1999.

Since the road segment was unbounded and the flume was in a natural drainage, visual observations were used to identify when there was additional runoff from upslope areas. Observations during most storm events indicated that the upslope areas only produced saturation overland flow during intense rainfall events with wet antecedent conditions. Similarly, subsurface flow interception by the cutslope on Maho-Road was short-lived and very rare (Ramos-Scharrón, 2004). Surface runoff from upslope areas or the cutslope was observed only on 12 November 1999, 17 November 1999, and 23 February 2000, and the runoff data from these three storms were excluded from the analysis.

During some runoff events one to six grab samples were collected in 250 ml plastic bottles at the flume outlet for determining suspended sediment concentrations. Over the 8-month study period, 70 samples were collected during 21 storm events; the limited number of grab samples is due to the unpredictability and brevity of natural rainfall events (median duration 15 min), and the difficulty of accessing the site during the more extreme storm events. Each sample was gravity-filtered through a preweighed 24 cm diameter ashless filter with a pore size of 3 μm, dried, and weighed to the nearest 0·01 g. The particle-size distributions of 46 samples collected during 18 storm events were determined by the hydrometer method (Gee and Bauder, 1986). The peak flow rates associated with these samples ranged from 0·03 to 14 cm h^{-1}.

A sediment fence 30 m downstream of the flume was used to obtain seven sediment yield measurements from Maho-Road between July 1998 and November 1999 (Ramos-Scharrón, 2004). Maho-Road was graded in both June 1998 and September 1999. For each measurement, all of the sediment was manually removed from the trap in 20 l buckets and weighed. A composite sample was collected to determine percentage moisture, and the measured moisture content was used to convert the field-measured wet weights to a dry mass. After drying, the particle-size distribution of this sample was determined by dry sieving (Bowles, 1992) for particles coarser than 0·075 mm and the hydrometer method (Gee and Bauder, 1986) for particles smaller than 0·075 mm. The overall mean particle-size distribution of the trapped sediment was calculated on a mass-weighted basis.

An empirical road erosion model (R&M model) was developed from the sediment fence data collected at the Maho-Road and 20 other road segments over a 2 year period. This model uses total precipitation, segment slope to the 1·5 power, and a categorical grading variable to predict sediment yields at the road segment scale (Ramos-Scharrón and MacDonald, 2005).

Infiltration modelling

Both of the runoff models developed in this study used a modification of the GA equation to predict infiltration. The GA equation is based on a one-dimensional approximation of Darcy's law. It assumes that piston flow creates a distinct wetting front, and that the suction head and hydraulic conductivity values are constant for a site (Scott, 2000). If the depth of ponding is assumed to be negligible, then the GA infiltration model can be expressed as

$$i(t) = K_s \left[\frac{h_f \Delta\theta_v}{I(t)} + 1 \right] \quad (1)$$

where $i(t)$ (cm h^{-1}) is infiltration capacity, K_s (cm h^{-1}) is the saturated hydraulic conductivity, h_f (cm) is the suction head, $I(t)$ (cm) is the cumulative depth of infiltration, and $\Delta\theta_v$ (cm^3 cm^{-3}) is the unfilled volumetric water content (Flerchinger and Watts, 1987) The $\Delta\theta_v$ term is the difference between the effective porosity of the soil, which is approximated by its water content at saturation (θ_{sat}), and the water content at the beginning of an individual storm event (θ_i). Precipitation excess was calculated for each 2·5- or 5-minute time step as the difference between the measured precipitation intensity and the predicted infiltration rate using Equation (1).

There were three main differences between the GA-UH and the GA-KW models in the use of the GA infiltration. First, infiltration over time was calculated for 5 min time steps in the GA-UH model and 2·5 min time steps for the GA-KW model, as these intervals yielded the best results. Second, the GA-UH model used a lumped hydraulic conductivity value ($K_{s\ road}$) for Maho-Road to calculate rainfall excess. In the GA-KW model, the suction head, initial water content, and saturated water content were treated as lumped parameters, but the saturated hydraulic conductivities for the partially paved (K_p) and unpaved (K_u) portions of Maho-Road were considered separately. The third difference is that the GA-UH model only allowed infiltration when it was raining, and the excess precipitation for each time step was automatically routed to the outlet of Maho-Road by the UH transform function. In contrast, the GA-KW model used a scaling parameter to calculate infiltration from the remaining overland flow after precipitation had ceased. This scaling parameter progressively reduces the

DOI: 10.1002/hyp

proportion of Maho-Road with overland flow as the runoff drains from each subsegment. The value of this parameter was derived from the estimated mean flow velocity and the length of each subsegment (Ramos-Scharrón, 2004).

The average infiltration rate for each event with reliable rainfall and runoff data was calculated by subtracting the total depth of runoff from the storm precipitation, and dividing this by the measured duration of runoff. These event-averaged infiltration rates were plotted against the duration of runoff, and a non-linear regression equation was fitted to these data to set the initial calibration values for $K_{s\ road}$, K_p, K_u, and the infiltration rate at the beginning of each storm event.

UH runoff modelling

A UH is an empirically defined function that transforms excess precipitation into an outflow hydrograph (McCuen, 1998). The UH approach assumes that the runoff hydrograph is linearly proportional to the amount of excess precipitation, and that the duration of the runoff hydrograph is constant for storms with the same duration (Gray, 1960). Hydrographs from eight storms were used to develop a 2·5 min UH following the rainfall-excess reciprocal method (Dunne and Leopold, 1978). The eight events were selected because they satisfied the requirements of the reciprocal method by having similar durations and single-peaked hydrographs. These criteria meant that the eight storms used to develop the UH all had relatively low amounts of runoff and short durations (Table II).

Six of these eight storms had runoff data with a 2·5 min resolution, whereas two storms (27 September 1999(c) and 4 January 2000) only had 5 min data. The S-hydrograph method was used to transform the 5 min UHs derived from these two storms into 2·5 min UHs (McCuen, 1998). The eight 2·5 min UHs were shifted so that each began at the same time relative to the beginning of excess rainfall. The final UH was constructed by calculating the mean runoff rate for each 2·5 min interval. No additional normalization was required, as the resulting UH represented 1 cm of precipitation excess.

Kinematic wave runoff modelling

Kinematic waves are a simplified version of the one-dimensional, distributed routing models described by the St Venant equations (Chow, 1998). Kinematic waves include the effect of momentum while neglecting the dynamic effects of pressure and acceleration. Hence, the movement of water over a plane can be defined by a momentum conservation formula, such as Manning's equation:

$$Q = \left(\frac{P^{2/3} S_o^{1/2}}{n}\right) A \tag{2}$$

where Q ($m^3\ s^{-1}$) is discharge, S_o ($m\ m^{-1}$) represents the water surface slope, n ($s\ m^{-1/3}$) is Manning's roughness coefficient, P (m) is the wetted perimeter of the flow, and A (m^2) is the cross-sectional flow area (Dunne and Leopold, 1978). The transfer of water from one plane to another uses a mass conservation equation:

$$q = \frac{\delta Q}{\delta x} + \frac{\delta A}{\delta t} \tag{3}$$

where x (m) is the downslope distance, t (s) is time, and q ($m^3\ s^{-1}$) represents the net inflows or outflows in the form of either precipitation or infiltration. A can be expressed as a power function of Q:

$$A = \alpha Q^{\beta} \tag{4}$$

where α and β are empirical coefficients (Chow, 1998). Equations (2) and (4) can be combined to calculate α, whereas β is normally set to 0·60 (Chow, 1998). After differentiating by time, Equations (3) and (4) can be combined to produce the kinematic flow equation:

$$q = \frac{\delta Q}{\delta x} + \left[\alpha\beta Q^{\beta-1}\left(\frac{\delta Q}{\delta t}\right)\right] \tag{5}$$

Since Q is the only dependent variable, all of the other parameters can be measured or estimated from the physical characteristics of the overland flow plane.

Equation (5) was solved for Maho-Road by following a backward linear difference method to approximate the time and space derivative of discharge (Chow, 1998). The solution to Equation (5) was used to calculate the discharge from each subsegment.

One difficulty of the kinematic wave approach is that discharge on the recession limb asymptotically approaches zero (Henderson and Wooding, 1964). This problem was resolved by forcing flows less than 0·03 cm h^{-1} to zero, as 0·03 cm h^{-1} is less than the minimum flow that could be measured with the flume.

Model calibration and validation

Model calibration required the simultaneous consideration of different parameters. The GA equation had three input parameters whose values needed to be calibrated ($K_{s\ road}$, h_f, $\Delta\theta_v$). The routing component of the GA-UH model used the empirical UH and required no further calibration. The GA-KW model required calibration of the hydraulic conductivity (K_u, K_p) and surface roughness (n_u, n_p) for the unpaved and partially paved subsegments, respectively.

Input parameters were adjusted to produce the best possible match between the predicted and observed hydrographs for the eight storms used to develop the UH (Table II). This calibration was done manually using a multi-objective calibration procedure. The three objective functions used for calibration and assessing model error were the percentage error in total discharge, percentage error in peak discharge, and the Nash–Sutcliffe coefficient of determination R^2_{NS} for the simulated hydrographs (Nash and Sutcliffe, 1970). R^2_{NS} was calculated for each event by

$$R^2_{NS} = \frac{\sum(q_i - \overline{q}_i)^2 - \sum(\hat{q}_i - q_i)^2}{\sum(q_i - \overline{q}_i)^2} \tag{6}$$

DOI: 10.1002/hyp

Table II. List of storms with reliable rainfall and runoff data in order of increasing precipitation. An asterisk indicates the events used for developing the UH and model calibration, and the remaining events were used for model validation

Event date	Total precipitation (cm)	Max. 5 min precipitation intensity (cm h^{-1})	Total discharge (cm)	Peak discharge (cm h^{-1})	Runoff coefficient	Antecedent precipitation index (cm)
13 Nov 99	0·28	2·44	0·119	1·09	0·43	11·2
27 Sep 99 (b)*	0·36	3·35	0·022	0·16	0·06	4·7
2 May 00	0·36	2·74	0·060	0·33	0·17	1·7
6 Nov 99	0·41	1·83	0·148	0·56	0·36	3·2
4 Jan 99*	0·41	2·40	0·013	0·05	0·03	4·3
20 Apr 00	0·43	2·44	0·011	0·05	0·03	0·8
13 Oct 99*	0·48	3·96	0·072	0·40	0·15	8·3
25 Oct 99	0·48	2·74	0·250	1·08	0·52	7·3
29 Apr 00*	0·53	4·88	0·045	0·50	0·08	0·6
12 Oct 99	0·58	2·44	0·151	0·24	0·26	6·8
27 Sep 99 (a)*	0·61	3·36	0·060	0·64	0·10	5·2
29 Jan 00*	0·61	3·36	0·016	0·10	0·03	0·7
14 Nov 99	0·69	2·13	0·067	0·52	0·10	11·6
22 Apr 00*	0·71	3·66	0·027	0·16	0·04	1·1
16 Nov 99	0·76	2·44	0·236	1·25	0·31	14·3
20 Oct 99	0·79	3·96	0·400	3·86	0·51	5·2
12 Sep 99	0·89	3·35	0·439	3·91	0·49	12·1
8 Sep 99	0·91	4·88	0·216	1·23	0·24	10·4
27 Sep 99 (c)	0·94	6·71	0·119	1·22	0·13	3·8
5 Oct 99*	0·94	7·92	0·144	1·77	0·15	5·5
6 Sep 99	1·04	4·27	0·312	1·34	0·30	9·2
10 Nov 99	1·24	4·57	0·363	1·50	0·29	2·2
30 Oct 99	2·31	7·92	0·842	4·22	0·36	5·7
5 Jan 00	2·36	6·71	1·47	6·25	0·62	4·7
11 Nov 99	2·74	7·62	1·98	10·90	0·72	3·5
23 Oct 99	2·84	12·80	2·04	11·20	0·72	7·2
Mean	0·95	4·42	0·370	2·10	0·28	5·8

where q_i is the measured discharge at time i, $\overline{q}_i$ is the mean runoff rate, and $\hat{q}_i$ is the predicted runoff at time i. An R^2_{NS} value of 1·0 indicates perfect agreement, whereas a negative value indicates that the model errors are greater than simply using the mean discharge. If the predicted runoff is zero, R^2_{NS} values cannot be calculated.

The GA-UH and GA-KW models were validated against measured runoff data from 18 storms. The three criteria used for calibration also were used to evaluate the performance of the calibrated GA-UH and GA-KW models.

Model application

The GA-UH and GA-KW models were used to estimate the total runoff from 2 September 1999 to 19 May 2000 for all storms with at least 0·07 cm of rainfall ($n = 160$). The predicted hydrographs from both models were combined with empirical sediment rating curves to estimate suspended sediment yields for the 160 storm events. The total sediment yield was divided by the amount of rainfall, and the resulting value was compared with both the sediment yield per centimetre of rainfall predicted for Maho-Road by the empirical R&M road erosion model (Ramos-Scharrón and MacDonald, 2005) and the yield rate measured by the sediment trap.

RESULTS AND DISCUSSION

Precipitation and runoff

There were 160 rainfall events between 2 September 1999 and 19 May 2000, and reliable runoff data were collected for 135 of these storms. The mean duration of the 160 rainfall events was 24 min and the duration of individual storms ranged from 5 to 295 min. The largest storm had 2·8 cm of precipitation and a maximum 5 min intensity of 12·8 cm h^{-1}.

Twenty-six of these 135 events produced runoff, with eight of these 26 storms being used for calibration and 18 storms being used for validation of the two runoff models. The total precipitation for these 26 runoff-producing events was 24·7 cm, and the total discharge was 9·6 cm or 39% of the rainfall (Table II). The median rainfall for the runoff-producing storms was 0·70 cm versus 0·10 cm for the 109 events that did not generate runoff. Storm discharge increased non-linearly with increasing storm rainfall ($r^2 = 0·94$) (Figure 3). At least 0·3 to 0·5 cm of rainfall and a 5 min intensity of 1·8 cm h^{-1} were required to initiate runoff. Runoff coefficients for storms with less than 1·3 cm of precipitation ranged from zero up to 0·52, whereas the runoff coefficients for storms larger than 2·2 cm ranged from 0·29 to 0·72 (Table II). The highest instantaneous peak discharge of 11·2 cm h^{-1} was recorded during a 2·8 cm storm that had the maximum 5 min rainfall intensity of 12·8 cm h^{-1}. Peak

DOI: 10.1002/hyp

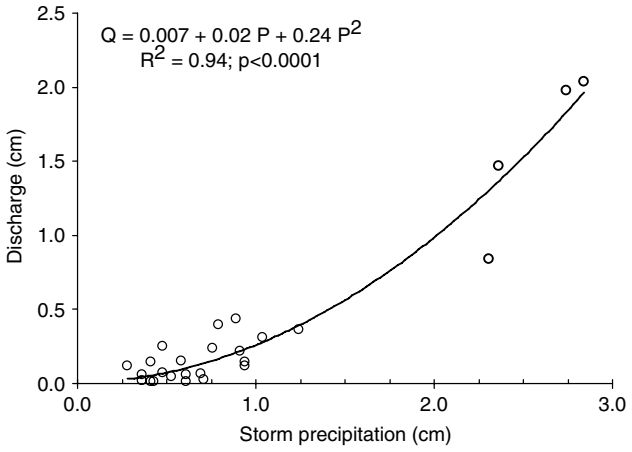

Figure 3. Relationship between storm precipitation (P) and discharge (Q) for the 26 events that produced runoff

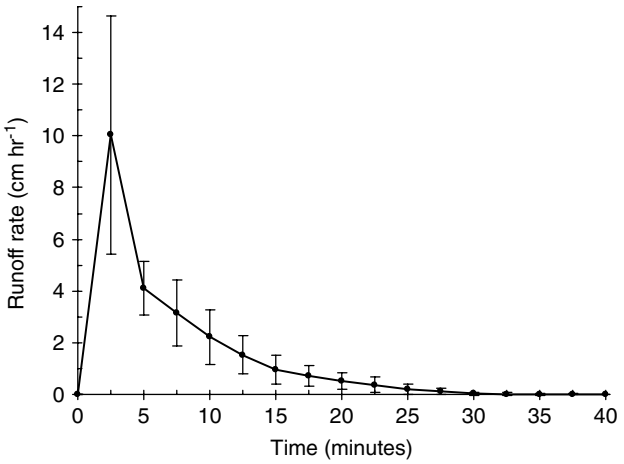

Figure 5. Mean 2·5 min UH for 1·0 cm of excess precipitation from Maho-Road. Bars indicate one standard deviation

flow rates were strongly related to total precipitation ($r^2 = 0{\cdot}81$) and the maximum 5 min precipitation intensity ($r^2 = 0{\cdot}60$).

The average infiltration rate for the 26 events that generated runoff was 1·2 cm h^{-1}, and the range was from 0·25 to 3·8 cm h^{-1}. The event-averaged infiltration rates were highly variable for the shorter duration runoff events, but after 40–50 min the event-averaged infiltration rate approached an asymptotic value of 0·4 cm h^{-1} (Figure 4). The inferred infiltration curve for Maho-Road declines sharply over time and approaches an asymptotic infiltration rate of 0·17 cm h^{-1} after about 20–30 min (Figure 4). This asymptotic value was used as the initial estimate of $K_{s\ road}$ in the GA model, and the initial infiltration rate was set to 3·25 cm h^{-1}.

The mean 2·5 min UH developed for the GA-UH model is shown in Figure 5. This has a time to peak of 2·5 min, a peak runoff rate of 10·0 cm h^{-1}, and a total duration of 37·5 min.

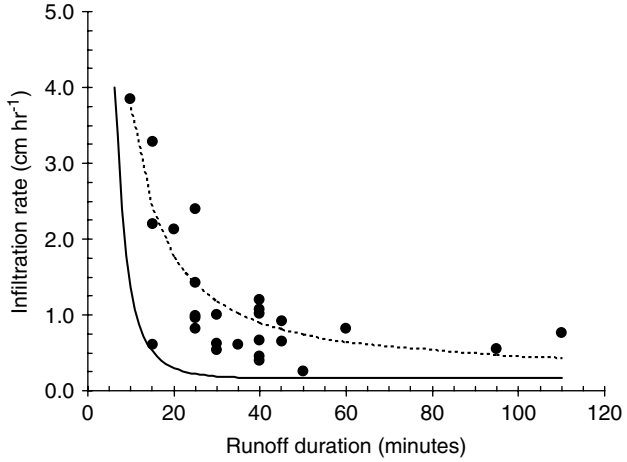

Figure 4. Relationship between duration of runoff and infiltration rates. Each point is the event-averaged infiltration rate calculated from one of the 26 events that produced runoff, and the dashed line identifies the non-linear regression that best describes this relationship ($r^2 = 0{\cdot}39$; $p < 0{\cdot}0001$). The solid line represents the inferred infiltration curve used to select the initial parameter values for the GA infiltration equation

Model calibration

Table III lists the allowed range of values for calibrating the two runoff models. The mean K_s for Maho-Road was allowed to vary from 0·12 to 0·25 cm h^{-1}, and the calibrated value for the GA-UH model was 0·20 cm h^{-1} (Table III). This value is consistent with data from other unpaved roads (Table IV). The saturated hydraulic conductivity K_p for the partially paved section of Maho-Road was determined by back-calculating its value based on the areally weighted $K_{s\ road}$ of 0·20 cm h^{-1} and the estimated hydraulic conductivity values for the unpaved sections K_u:

$$K_p = 1{\cdot}33 - 5{\cdot}66K_u \quad (7)$$

The saturated hydraulic conductivity of the unpaved segments K_u was varied from 0·20 to 0·24 cm h^{-1} to keep K_p greater than zero but less than K_u. The final hydraulic conductivity values for the GA-KW model were 0·23 cm h^{-1} for K_u and 0·020 cm h^{-1} for K_p.

The suction head was varied from 2·0 to 8·0 cm, as this was the range of values found by Flerchinger and

Table III. Range of parameter values considered in model calibration and the final calibrated values for the GA-UH and GA-KW models (subscripts 'u' and 'p' refer to the partially paved and unpaved subsegments respectively; NA indicates not applicable)

Parameter	Range of possible values	Model	
		GA-UH	GA-KW
$K_{s\ road}$ (cm h^{-1})	0·12–0·25	0·20	NA
K_u (cm h^{-1})	0·20–0·24	NA	0·23
K_p (cm h^{-1})	0·00–0·22	NA	0·02
Maximum infiltration rate (cm h^{-1})	0–∞	3·25	3·25
h_f (cm)	2·0–8·0	7·0	7·0
$\Delta\theta_v$ ($cm^3\ cm^{-3}$)	0·25–0·60	0·35	0·35
θ_s ($cm^3\ cm^{-3}$)	0·35–0·70	0·45	0·45
θ_i ($cm^3\ cm^{-3}$)	0·10	0·10	0·10
Manning's n_u (s $m^{-1/3}$)	0·010–0·030	NA	0·024
Manning's n_p (s $m^{-1/3}$)	0·010–0·013	NA	0·010
β	0·60	NA	0·60

DOI: 10.1002/hyp

Table IV. Summary of previous hydrologic and sediment data for unpaved roads (dashes indicate no data)

Reference	Spatial scale	Runoff coefficient (cm cm^{-1})	Average infiltration (cm h^{-1})	Hydraulic conductivity (cm h^{-1})	Sediment concentration (mg l^{-1})	Sediment by size categories
Bilby *et al*. (1989)	Segment (700–3600 m^2)	—	—	—	70–10 000	80% clays, 20% silt and coarser
Bren and Leitch (1985)	Segment (2100 m^2)	0·04–0·80	—	—	—	—
Coker *et al*. (1993)	Subsegment (35–60 m^2)	0·42–0·66	—	—	3 000–130 000	—
Fahey and Coker (1992)	Subsegment (100 m^2)	—	0·3	—	3 000	85% silts and clays, 15% sand and coarser
Grayson *et al*. (1993)	Segment (~1100 m^2)	—	—	—	23 000–40 000	66% fines, 33% coarse
Harden (1992)	Sub-plot (0·02 m^2)	0·00–1·0	0·4–3·6	—	520–227 000	—
Kahklen (1994)	Segment (100–250 m^2)	—	0·09	—	0·2–118	—
Luce (1990), Luce and Cundy (1992)	Plot (1 m^2)	—	—	0·17–0·60	—	—
Luce and Cundy (1994)	Plot (1–5 m^2)	—	—	0·21–0·50	—	—
Reid (1981), Reid and Dunne (1984)	Segment (250–920 m^2)	0·44–0·58	0·05	—	70–30 000	—
Sampson (1999), MacDonald *et al*. (2001)	Subsegment (35–60 m^2)	0·04–0·13	—	—	5 000–50 000	4–40% silts and clays, 60–96% sand and coarser
Vincent (1979)	Segment (110–160 m^2)	0·37–0·80	0·02–0·05	—	—	—
Wald (1975)	Segment (400–800 m^2)	—	—	—	100–1 300	—
Ziegler and Giambelluca (1997)	Sub-plot (<1 m^2)	0·02–0·88	—	0·02–0·5	—	—
Ziegler *et al*. (2000)	Plot (~3 m^2)	0·62–0·84	0·62–3·7	—	—	—
Ziegler *et al*. (2001b)	Plot (~3–5 m^2)	0·60–0·86	0·62–1·6	—	25 000–68 000	—

Watts (1987) for unpaved roads in the western USA. The calibrated value for both models was 7·0 cm. The unfilled volumetric water content $\Delta\theta_v$ was considered as a single calibration parameter because model performance did not improve when the initial water content θ_i was varied according to the 6 h or 24 h antecedent precipitation, or the antecedent precipitation index. $\Delta\theta_v$ was allowed to vary between 0·25 and 0·60 cm^3 cm^{-3}, and the calibrated value of 0·35 cm^3 cm^{-3} presumes that θ_i is equal to 0·10 cm^3 cm^{-3} and θ_s is 0·45 cm^3 cm^{-3} (Table III). The θ_s value of 0·45 cm^3 cm^{-3} is slightly outside the range of 0·25–0·40 cm^3 cm^{-3} that was back-calculated from bulk density samples taken from unpaved roads in the western USA (Helvey and Kochenderfer, 1990).

Manning's roughness coefficient for the unpaved sections (n_u) was allowed to vary from 0·010 to 0·030 s m$^{-1/3}$, and the value for the partially paved section (n_p) was allowed to vary from 0·010 to 0·013 s m$^{-1/3}$ (Woolhiser, 1975). The calibrated values used in the GA-KW model were 0·024 s m$^{-1/3}$ for n_u and 0·010 s m$^{-1/3}$ for n_p (Table III).

Model validation

The mean amount of runoff for the 18 storms used to validate the two runoff models was 0·51 cm, and the range was from 0·013 to 2·04 cm (Tables II and V). The mean absolute errors in predicted runoff for the two models were 0·16 and 0·17 cm, or slightly more than 30%. Both models tended to underpredict the amount of runoff, as the mean observed runoff coefficient was 0·36 and the mean predicted runoff coefficient was 0·26 for the GA-UH model and just slightly lower at 0·24 for the GA-KW model.

The models did a relatively poor job of predicting total storm discharge for the smaller events, but their relative performance improved with increasing discharge (Figure 6a). The models predicted no runoff for almost half of the 14 events with less than 0·5 cm of runoff. For the four storms with at least 0·5 cm of runoff, the models had a mean absolute error of 0·25 cm, or just 16% in relative terms (Table V).

A similar pattern was observed for the R^2_{NS} values (Figure 6b). The overall mean R^2_{NS} values were 0·31 for the GA-UH model ($n = 13$ storms) and 0·39 for the GA-KW model ($n = 12$ storms) (Table V). For events with less than 0·5 cm of runoff, the mean R^2_{NS} values were 0·21 and 0·29 for the GA-UH and GA-KW models respectively. For events with at least 0·5 cm of runoff, the mean R^2_{NS} values increased to 0·54 for the GA-UH model and 0·61 for the GA-KW.

Both models were generally able to predict the timing of the peak flow to within 2·5 min of the observed

DOI: 10.1002/hyp

Table V. Summary of validation results for the GA-UH and GA-KW models (NA indicates not applicable; SD indicates standard deviation; absolute mean errors are indicated by an asterisk)

Event	Observed			GA-UH model						GA-KW model					
	Runoff (cm)	Runoff coefficient (cm cm^{-1})	Peak flow (cm h^{-1})	Predicted runoff (cm)	Error in runoff (cm)	Runoff coefficient (cm cm^{-1})	Peak flow (cm h^{-1})	Error in peak flow (cm h^{-1})	R^2_{NS}	Predicted runoff (cm)	Error in runoff (cm)	Runoff coefficient (cm cm^{-1})	Peak flow (cm h^{-1})	Error in peak flow (cm h^{-1})	R^2_{NS}
20 Apr 00	0·01	0·03	0·05	0·00	−0·01	0·00	0·00	−0·05	NA	0·00	−0·01	0·00	0·00	−0·05	NA
2 May 00	0·06	0·17	0·33	0·00	−0·06	0·00	0·00	−0·33	NA	0·00	−0·06	0·00	0·00	−0·33	NA
14 Nov 99	0·07	0·10	0·52	0·06	−0·01	0·09	0·27	−0·25	0·45	0·00	−0·07	0·00	0·00	−0·52	NA
13 Nov 99	0·12	0·42	1·09	0·00	−0·12	0·00	0·00	−1·09	NA	0·00	−0·12	0·00	0·00	−1·09	NA
27 Sep 99 (c)	0·12	0·13	1·22	0·36	0·24	0·39	2·04	0·82	−1·54	0·32	0·20	0·34	1·10	−0·12	−0·36
6 Nov 99	0·15	0·36	0·56	0·00	−0·15	0·00	0·00	−0·56	NA	0·00	−0·15	0·00	0·00	−0·56	NA
12 Oct 99	0·15	0·26	0·24	0·00	−0·15	0·00	0·00	−0·24	NA	0·00	−0·15	0·00	0·00	−0·24	NA
8 Sep 99	0·22	0·24	1·23	0·33	0·11	0·36	1·72	0·49	0·41	0·30	0·09	0·33	1·26	0·03	0·71
16 Nov 99	0·24	0·24	1·25	0·15	−0·09	0·17	0·51	−0·74	0·43	0·08	−0·15	0·08	0·17	−1·08	0·11
25 Oct 99	0·25	0·52	1·08	0·01	−0·24	0·02	0·08	−1·00	−0·07	0·00	−0·25	0·00	0·04	−1·04	0·02
6 Sep 99	0·31	0·30	1·34	0·41	0·10	0·40	2·01	0·67	0·70	0·38	0·07	0·37	1·36	0·02	0·84
10 Nov 99	0·36	0·29	1·50	0·34	−0·03	0·27	1·94	0·44	0·68	0·30	−0·06	0·26	1·07	−0·43	0·62
20 Oct 99	0·40	0·51	3·86	0·20	−0·20	0·26	1·41	−2·45	0·49	0·15	−0·25	0·19	0·70	−3·16	0·19
12 Sep 99 (b)	0·44	0·49	3·91	0·15	−0·29	0·17	1·02	−2·89	0·36	0·13	−0·31	0·16	0·52	−3·39	0·16
30 Oct 99	0·84	0·36	4·22	1·43	0·59	0·62	4·87	0·65	0·21	1·39	0·54	0·60	4·66	0·44	0·30
5 Jan 00	1·47	0·62	6·25	1·56	0·09	0·66	5·04	−1·21	0·68	1·51	0·05	0·64	5·01	−1·24	0·82
11 Nov 99	1·99	0·72	10·86	1·68	−0·30	0·61	4·68	−6·18	0·60	1·61	−0·38	0·59	4·38	−6·48	0·59
23 Oct 99	2·04	0·72	11·24	2·02	0·02	0·71	6·52	−4·72	0·66	1·97	−0·07	0·69	5·95	−5·29	0·74
Sum	9·23	NA	NA	8·71	NA	NA	NA	NA	NA	8·15	NA	NA	NA	NA	NA
Mean	0·51	0·36	NA	0·48	0·16*	0·26	NA	1·38*	0·31	0·45	0·17*	0·24	NA	1·42*	0·39
SD	0·64	0·21	NA	0·68	0·14	0·25	NA	1·67	0·60	0·66	0·14	0·25	NA	1·90	0·38

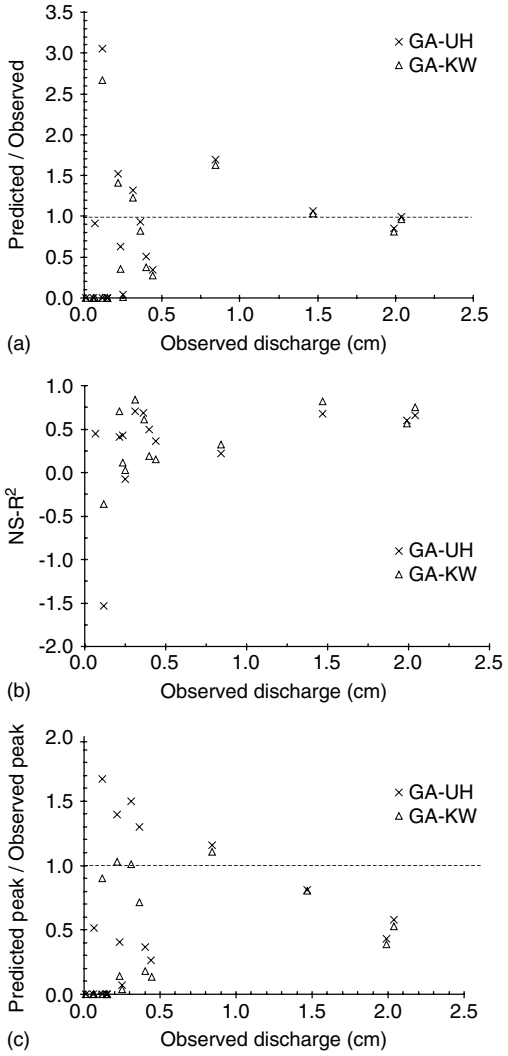

Figure 6. Performance of the GA-UH and GA-KW models for the 18 storms used for validation. (a) Observed discharge versus the ratio of predicted to observed discharge. The dotted line indicates perfect agreement. (b) Nash–Sutcliffe coefficient of determination R^2_{NS} versus total discharge. (c) Ratio of predicted to observed peak runoff rates versus total discharge. The dotted line indicates perfect agreement

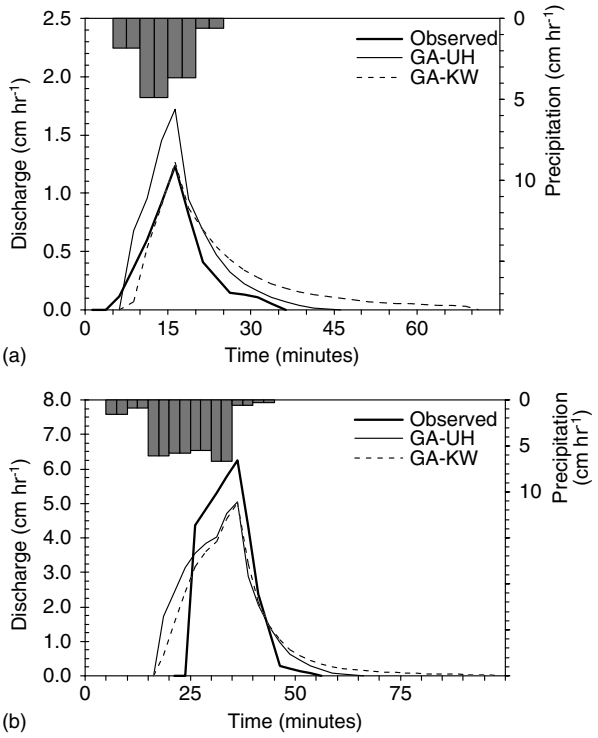

Figure 7. Hyetograph, observed hydrograph, and simulated hydrograph for: (a) 0·91 cm storm on 8 September 1999; (b) 2·36 cm storm on 5 January 2000

value, but they were much less accurate in predicting the magnitude of peak flows. The mean absolute difference between the predicted and observed peak flows was about 1·4 cm h^{-1} for the two models (Table V). The GA-UH model tended to predict slightly higher peak flows than the GA-KW model. In contrast to the other criteria, the accuracy of the predicted peak flows did not greatly improve with increasing storm discharge in either absolute or relative terms (Figure 6c).

Figure 7 illustrates model performance by comparing the observed and predicted hydrographs for a 0·91 cm storm on 8 September 1999 and a 2·36 cm storm on 5 January 2000. For the first storm the GA-KW model and the GA-UH model overpredicted the amount of runoff by 40–50%, with the GA-KW model producing a larger and longer recession limb than was observed (Figure 7a). The GA-UH model overpredicted the observed peak flow of 1·23 cm h^{-1} by 40%, whereas the GA-KW model overpredicted the peak flow by only 3% (Table V). The R^2_{NS} value of 0·71 for the GA-KW model was substantially better than the R^2_{NS} value of 0·41 for the GA-UH model. For the second, larger storm the model performance was slightly better, as each model overpredicted the amount of runoff by less than 6% and underpredicted the peak flow by slightly less than 20% (Figure 7b). The R^2_{NS} value of 0·82 for the GA-KW model was substantially better than the R^2_{NS} of 0·68 for the GA-UH model (Table V).

The results suggest that the GA-KW model generally performs slightly better than the GA-UH model, but it has a slightly greater tendency to underpredict peak flow rates (Table V). For both models, the predicted hydrographs tended to last longer than the observed hydrographs. The errors in the predicted runoff hydrographs can be attributed primarily to problems in calculating precipitation excess rather than problems in runoff routing. The difficulty in accurately predicting the initial infiltration rate is shown by the fact that both models generally predicted no runoff when the measured runoff was less than 0·15 cm (Figure 6a), and both models tended to underestimate the amount of runoff from smaller events. This difficulty is not surprising given the wide variation in runoff coefficients for storms with less than 1 cm of precipitation (Figure 3; Table II). Since the maximum 5 min storm intensity was not significantly correlated with the runoff coefficients for these smaller events ($r^2 = 0{\cdot}04$), the variability in the runoff coefficients must be attributed to the variability in the initial infiltration rates. Figure 4 shows that the mean infiltration rate was highly variable for the smaller events, but it was not possible to define

DOI: 10.1002/hyp

an infiltration rate for events shorter than 10 min because this was the minimum time of concentration (i.e. the time needed for water from the most distant portion of Maho-Road to reach the flume).

In general, the GA model tended to underestimate runoff for these smaller events, and the results suggest that the calibrated model may compensate for underestimating runoff during the beginning of an event by underpredicting infiltration rates during the recession limb of the storm hydrographs. The net result is that the predicted hydrographs are too responsive to precipitation intensity in the latter portion of the hydrographs and that runoff continues for longer than what was observed. Attempts to correct this problem by dropping the initial infiltration rate to less than 3·25 cm h^{-1} made it difficult to calibrate the GA model. The relatively high errors in the predicted runoff for smaller storms can be attributed to the fact that runoff is a small difference between two much larger numbers (precipitation and infiltration). Hence, the predicted runoff is extremely sensitive to the predicted infiltration. Given these issues and the inability of the models to account for the variation in initial infiltration rates, it is not surprising that the models were not able to predict the amount of runoff accurately for the smaller events. Similar problems have been identified by other studies that have attempted to develop and test rainfall–runoff models for unpaved roads, including some strictly controlled experiments on small plots using rainfall simulators (Simons *et al.*, 1978; Luce, 1990; Luce and Cundy, 1994).

Although the models were better able to predict the amount of runoff for the larger events, the models greatly underpredicted the peak flows in most of the larger events (Table V). The inability to predict peak flows accurately also stems from the inability of the GA model to predict infiltration rates accurately during the initial stages of precipitation events. For the 18 validation events, the median time from the beginning of precipitation to the observed peak flow was only 10 min, and the range was from 5 to 30 min. Since these times generally are less than the 30 min required for infiltration to reach its asymptotic value (Figure 4), the problems in predicting the initial infiltration rates are largely responsible for the errors in predicting both peak flows and total runoff.

In practical terms, the errors in predicted discharge for the smaller events are relatively unimportant, as the 14 smallest events in Table II produced only 11% of the total runoff. The four largest events listed in Table II accounted for nearly two-thirds of the total runoff, and the models did a much better job of predicting the amount of runoff for these larger events (Figure 6a).

The calibrated GA-UH and GA-KW models were used to estimate runoff from the 160 storms with at least 0·07 cm of precipitation that occurred between 2 September 1999 and 19 May 2000. Some ninety percent of these events had less than 1·0 cm of rainfall, and these accounted for only 49% of the total rainfall (Figure 8). An analysis of the long-term rainfall data at Caneel Bay confirms that storms with less than 1·0 cm

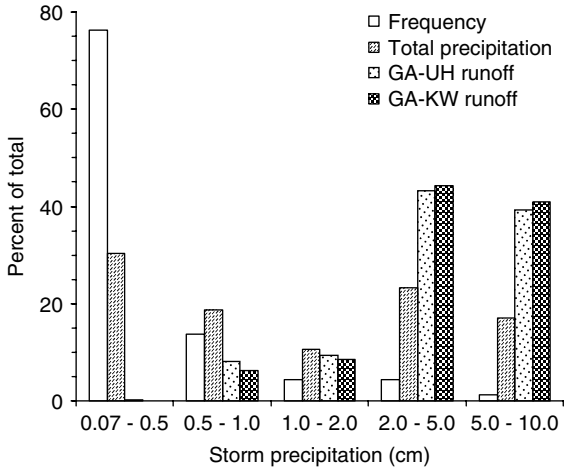

Figure 8. Relative frequency of storms, storm precipitation, and predicted runoff by storm size for 160 storms at Maho-Road between 2 September 1999 and 19 May 2000

of precipitation represent nearly 90% of all storms, but account for slightly less than half of the total rainfall (Ramos-Scharrón, 2004).

The GA-UH model predicted 29·7 cm of runoff from these 160 storm events, or 35% of the total precipitation (Figure 8), whereas the runoff predicted from the GA-KW model was slightly lower at 27·9 cm. Both models estimated that 92% of the total runoff would come from the 10% of storms with more than 1·0 cm of rainfall. The two storms with at least 5 cm of rainfall accounted for 17% of the total rainfall and 40% of the predicted runoff (Figure 8).

Sediment concentrations and sediment yields

The mean suspended sediment concentration for the 70 grab samples taken at Maho-Road was 20 800 mg l^{-1} (SD = 17 800 mg l^{-1}), and the range was from 1270 to 84 400 mg l^{-1}. These values are consistent with the results from most other road erosion studies (Table IV). Suspended sediment concentrations rapidly increased with discharge at low runoff rates, but there was not a clear relationship between discharge and suspended sediment concentrations once runoff rates exceeded approximately 0·5 cm h^{-1} (Figure 9).

Some of the variability in Figure 9 is due to the fact that Maho-Road was regraded on 10 September 1999, and the 27 samples collected over eight storms from 12 September to 25 October 1999 generally had much higher suspended sediment concentrations. The mean concentration for these 27 samples was nearly 30 000 mg l^{-1}, or almost twice the mean concentration of the remaining 43 samples, even though both periods had similar distributions of storm sizes, rainfall intensities, and peak flows. Hence, separate sediment rating curves were developed for the samples not affected by grading (Equation (8a)) and the samples collected in the first 6 weeks after grading (Equation (8b)):

$$C_{o\ \text{ungraded}} = 19\,000Q^{0.34}\ (R^2 = 0{\cdot}40;\ p < 0{\cdot}0001) \quad (8a)$$

$$C_{o\ \text{graded}} = 31\,100Q^{0.48}\ (R^2 = 0{\cdot}35;\ p = 0{\cdot}011) \quad (8b)$$

DOI: 10.1002/hyp

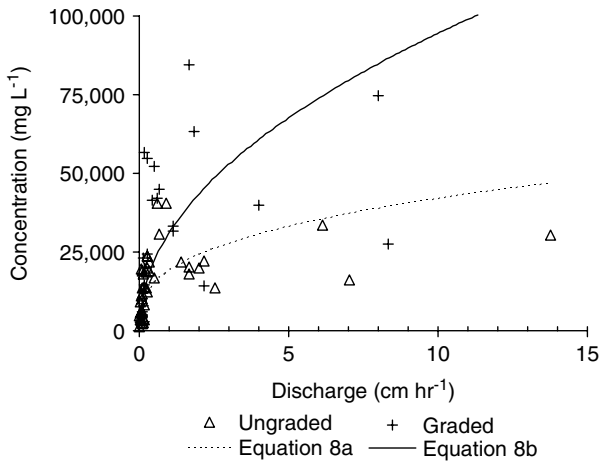

Figure 9. Relationship between suspended sediment concentrations and discharge for Maho-Road. Maho-Road was graded on 10 September 1999, and the data from 12 September to 25 October 1999 are plotted using a plus sign

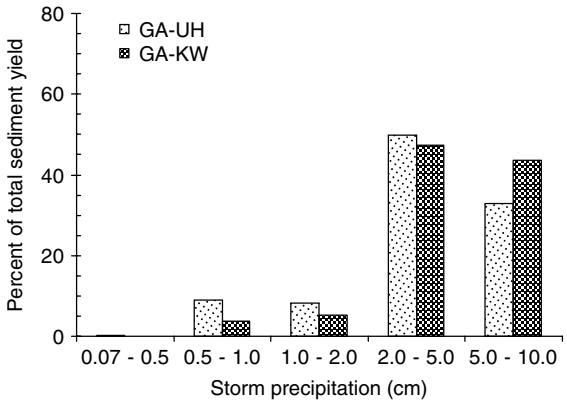

Figure 10. Relative frequency of predicted sediment yields by storm size for 160 storms between 2 September 1999 and 19 May 2000

where C_o (mg l^{-1}) is the suspended sediment concentration and Q (cm h^{-1}) is the instantaneous runoff rate. The development of two sediment rating curves is supported by differences in the particle-size distribution of the sediment samples.

The mass-weighted particle-size distribution of the 27 samples that were not affected by grading was 22% sand (0·062–2·00 mm), 70% silt (0·004–0·062 mm), and 8% clay (<0·004 mm). The relative percentages of sand, silt, and clay were highly variable, and there was not a clear relationship between discharge and the particle-size distribution. For the 19 samples collected within the first 6 weeks after grading, the mass-weighted particle-size distribution was much coarser at 65% sand, 34% silt, and only 1% clay. Although the particle-size distribution of the material used to grade the road is not known because it was a combination of native and imported material, it is assumed to be dominated by sand-sized particles, as evidenced by the post-grading increase in sand production.

Sediment yield models and model comparisons

The GA-UH and GA-KW models were coupled with Equation (8b) to estimate the total sediment yield during the first 6 weeks after grading, and with Equation (8a) to estimate the sediment yield from all other storm events between 2 September 1999 and 19 May 2000. The estimated sediment yields from Maho-Road for the entire study period were 12·3 Mg for the GA-UH model and 11·3 Mg for the GA-KW model. The distribution of predicted sediment yields by storm size (Figure 10) is very similar to the predicted proportions of runoff (Figure 8), as the 11 storm events with more than 1·0 cm of rainfall accounted for less than half of the total rainfall but 95% of the total sediment yield. The two storms with more than 5 cm of rainfall accounted for 17% of the total rainfall while producing 42% of the total sediment yield (Figure 10). The GA-UH model predicted a slightly higher sediment yield because the GA-UH model predicted higher peak flows and slightly more runoff, particularly for the larger events that generated most of the predicted sediment yield.

The predicted sediment yields for Maho-Road convert to approximately 140 kg of sediment per centimetre of rainfall, or 0·11 kg per square metre of road surface per centimetre of rainfall (kg m^{-2} cm^{-1}). When normalized by precipitation, the predicted sediment yield for the 6-week period following grading is about 150 kg per centimetre of rainfall, or only 7% higher than the rate for periods unaffected by grading. This small difference is due to the lack of large storms with high runoff rates.

These predicted sediment yields can be compared to the predicted sediment yield from Maho-Road using the empirical R&M model and the measured sediment yield from the sediment trap below Maho-Road (Ramos-Scharrón and MacDonald, 2005). Using the R&M model, the predicted sediment yield for Maho-Road for the 8-month study period is 150 kg per centimetre of precipitation (0·12 kg m^{-2} cm^{-1}), or only 10% higher than the yields predicted from the coupled runoff models and Equations (8a) and (8b). Eight of the 21 road segments used to develop the R&M model had sufficient sediment trap data to show that grading increased sediment production rates. The data from these eight segments suggest that, after grading, sediment production rates decline exponentially when plotted against cumulative rainfall (Ramos-Scharrón and MacDonald, 2005). The resultant empirical relationship is:

$$\mathrm{Er} = -0{\cdot}37 \ln\left(\sum P\right) + 2{\cdot}8 \qquad (9)$$

where Er is the sediment production rate for a road segment in kilograms per square metre of road surface per centimetre of rainfall per unit slope (m m^{-1}), and $\sum P$ is the cumulative rainfall in centimetre since the segment was graded ($r^2 = 0{\cdot}21$). If Equation (9) is applied to the unpaved subsegments of Maho-Road for the 22 cm of rainfall that fell in the first 6 weeks after grading, then the predicted sediment yield is 4040 kg or 0·15 kg m^{-2} cm^{-1}, which is 22% more than the sediment yield estimated for the same time period by the runoff models and Equation (8b).

DOI: 10.1002/hyp

Data from the Maho-Road sediment trap indicate an average sediment yield of 340 kg per centimetre of rainfall (0·27 kg m^{-2} cm^{-1}) between June 1998 and November 1999. This rate is 2·4 times higher than the coupled runoff–sediment yield models and 2·3 times higher than the R&M model (Figure 11). The difference in sediment yields between the coupled runoff–sediment rating curve models and the Maho-Road sediment trap data may be attributed in large part to the bias in their respective abilities to measure different particle sizes. For the suspended sediment samples, silts and clays accounted for 59% of the total mass and there were no particles larger than 2 mm. In contrast, silts and clays accounted for only 7% of the total mass captured in the sediment trap and particles larger than 2 mm accounted for 44% of the total sediment yield (Figure 12).

The particle-size distributions in Figure 12 show that the grab samples taken at the flume do a poor job of capturing the coarser particles. This bias is due to the intermittent transport of coarse particles and their non-uniform distribution within the flow cross-section (Edwards and Glysson, 1988). There is also some bias because the coarser particles were probably produced during the most intense storm events, when it was difficult to access the site and collect samples. Conversely, sediment traps are more efficient in capturing the larger particles because these settle out more quickly (Ice, 1986; Robichaud and Brown, 2002). Finer particles are more likely to be transported out of the trap with the excess runoff once the sediment trap is filled with water, and this bias increases as the sediment trap fills with sediment and the detention time decreases.

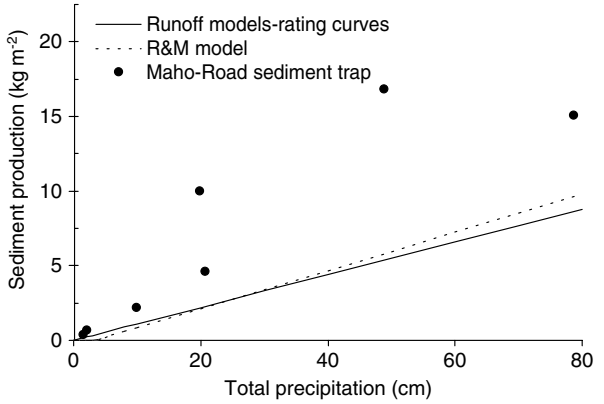

Figure 11. Relationship between total precipitation, measured sediment production rates using the sediment trap below Maho-Road, and predicted sediment production using the GA-UH model, GA-KW model, and R&M empirical road-segment model, respectively

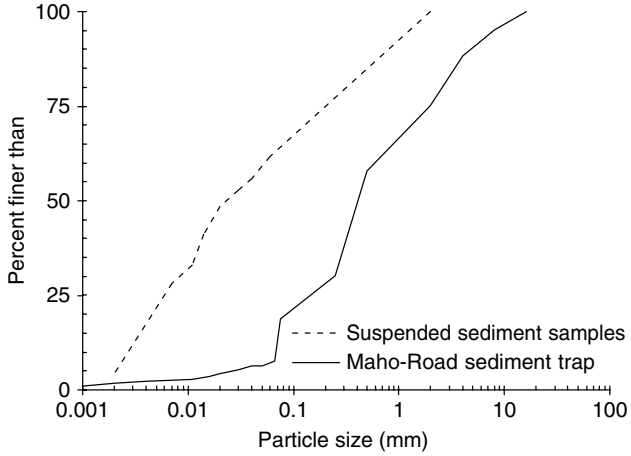

Figure 12. Mass weighted particle-size distribution for the suspended sediment samples and the material collected from the Maho-Road sediment trap

Since each method was more efficient at collecting a different particle-size distribution, the actual sediment production rate from Maho-Road is almost certainly higher than either estimate. If the suspended sediment data over the 8-month study period are used to estimate the production of silt and clay, and the sediment trap data are used to estimate the production of sand and gravel, then the total sediment production rate is about 390 kg per centimetre of rainfall, or 0·31 kg m^{-2} cm^{-1}. This is about 2·8 times higher than the sediment production rates estimated by the two runoff–sediment rating curve models, 2·6 times higher than the values estimated by the R&M model, and 15% higher than the measured value from the Maho-Road sediment trap. The combined data suggest that the sediment eroded from Maho-Road will consist of approximately 36% gravel, 44% sand, 19% silt, and 1% clay. Since gravel- and sand-sized particles comprise over 80% of the total sediment yield from Maho-Road, it follows that the sediment trap will provide better estimates of the total sediment yield than the coupled runoff–sediment rating curve models.

Relatively few studies have examined the particle-size distribution of the material eroded from unpaved roads, but the limited data suggest that the material being eroded from Maho-Road is unusually coarse textured (Table IV). In New Zealand, the sediment from unpaved roads in areas dominated by silty clays and silty-clay loams was 85% silt and clay (Fahey and Coker, 1992). In Australia, about two-thirds of the annual sediment production from roads was collected by Coshocton wheels and assumed to be transported as suspended sediment, while one-third was coarse material captured in a sediment collection flume (Grayson *et al.*, 1993). The much higher proportion of coarse material from Maho-Road can be attributed in part to the high rainfall intensities and exceptionally high runoff rates. It is less clear why the estimated proportion of clay is substantially less than the amount of clay in the gravelly loam soils in the Maho Bay area. The low percentage of clay in the eroded sediment may be due to the composition of the material used in grading the road surface, as this commonly includes moderately weathered bedrock that is scraped from the road cutslopes as well as material brought in from other areas on St John.

These results show that different measurement techniques can yield widely varying particle-size distributions and sediment production rates. Future studies should consider combining measurement approaches to more accurately capture the entire particle-size distribution of the sediment being produced, and thereby

DOI: 10.1002/hyp

generate more accurate estimates of sediment production rates. An accurate characterization of the eroded sediment is also essential for routing the material through the stream network and predicting downstream effects (Reid and Dunne, 1996; Bunte and MacDonald, 1999).

The revised erosion rate of 0·31 kg m^{-2} cm^{-1} for Maho-Road converts to 36 kg m^{-2} $year^{-1}$, assuming a mean annual rainfall of 115 cm. This road erosion rate is high relative to nearly all other road erosion studies (Ramos-Scharrón and MacDonald, 2005). This high rate can be attributed to the high rainfall intensities and runoff rates on St John, as well as to the relatively high traffic load in and out of the Maho Bay Eco Resort. The sediment production rate for Maho-Road also is four orders of magnitude higher than the sediment production rate from undisturbed hillslopes (MacDonald *et al*., 2001; Ramos-Scharrón, 2004). The implication is that unpaved roads are likely to be the dominant sediment source in areas with even a moderate density of unpaved roads.

A final lesson from this study is that very small storms do generate surface runoff and erosion from unpaved roads, but it is the largest storm events that generate most of the road-related sediment. The improved understanding of road runoff and erosion processes generated by this study should improve future modelling efforts and help guide road drainage design. Better estimates of road runoff and erosion rates are needed to guide future development and minimize the production and delivery of sediment from unpaved roads. The high road erosion rates documented in this study show that actions are needed to reduce the potential adverse effects of unpaved roads on the near-shore marine ecosystems that are so important to coastal communities.

CONCLUSIONS

Precipitation and runoff data were collected from 135 storms on a 230 m long road segment on the island of St John in the eastern Caribbean. Only 0·3 to 0·5 cm of precipitation was needed to initiate runoff, and runoff was generated from just 26 of the 135 storms. The calculated mean infiltration rate for the 26 events that produced runoff was 1·2 cm h^{-1}, and the range was from 0·25 to 3·8 cm h^{-1}.

Precipitation and runoff data from eight events were used to develop and calibrate two runoff models. The first model (GA-UH) predicted runoff using the GA infiltration equation and an empirically derived unit hydrograph. The second model (GA-KW) routed runoff using a kinematic wave approach. The validation data showed that the two models had a similar performance, as the mean Nash–Sutcliffe coefficient of determination was 0·31 for the GA-UH model and 0·34 for the GA-KW model. Much of the error in the predicted hydrographs was attributed to the inability of the models to capture the variability in the initial infiltration rates.

Suspended sediment concentrations increased nonlinearly with discharge, and the mean suspended sediment concentration from 70 grab samples was 20 800 mg l^{-1}. Sediment concentrations doubled for a 6-week period after the segment was graded, and this necessitated the development of two sediment rating curves.

The runoff models were coupled with the sediment rating curves to predict runoff and sediment production from Maho-Road for an 8-month period. The results showed that the storm events larger than 1·0 cm accounted for just less than half of the total precipitation, but produced about 90% of the total runoff and sediment yield. When normalized by precipitation and road surface area, the predicted sediment yields were about 0·11 kg m^{-2} cm^{-1}. This rate is only about 8% less than the 0·12 kg m^{-2} cm^{-1} estimated by a general road erosion model, but it is only 40% of the sediment yield measured from a sediment trap placed immediately below Maho-Road. Since the suspended sediment data did not adequately sample the coarse particles and the sediment trap was not effective in capturing the smaller particles, the combined data suggest a sediment yield from Maho-Road of 0·31 kg m^{-2} cm^{-1}, or about 36 kg m^{-2} $year^{-1}$. This rate is four orders of magnitude higher than the sediment yields measured from undisturbed zero-order basins, thereby confirming that unpaved roads are a very important sediment source. The improved understanding of runoff and erosion processes can help minimize the production and delivery of sediment from unpaved roads. The event-based models developed here can help improve the predictions of road runoff and road surface erosion on St John and in other areas, and thereby help guide future development.

ACKNOWLEDGEMENTS

This study was supported by the Water Resources Division of the National Park Service, the Water Resources Research Institute of the University of the Virgin Islands, and the Virgin Islands Department of Planning and Natural Resources. We gratefully acknowledge the logistical support provided by the Island Resources Foundation and the Virgin Islands National Park. We would also like to thank Professor Ellen Wohl, Professor Denis Dean, Dr William Jackson, and two anonymous reviewers for their valuable comments on the manuscript.

REFERENCES

Anderson B, Potts DF. 1987. Suspended sediment and turbidity following road construction and logging in western Montana. *Water Resources Bulletin* **23**: 681–690.

Anderson DM. 1994. *Analysis and modeling of erosion hazards and sediment delivery on St. John, U.S. Virgin Islands*. Technical Report NPS/NRWRD/NRTR-94-34, US National Park Service Water Resources Division, Fort Collins, CO.

Anderson DM, MacDonald LH. 1998. Modelling road surface sediment production using a vector geographic information system. *Earth Surface Processes and Landforms* **23**: 95–107.

Bilby RE, Sullivan K, Duncan SH. 1989. The generation and fate of road-surface sediment in forested watersheds in southwestern Washington. *Forest Science* **35**(2): 453–468.

Borga M. Tonelli F, Selleroni J. 2004. A physically based model of the effects of forest roads on slope stability. *Water Resources Research* **40**: W12202. DOI: 10·1029/2004WR003238.

Bowden MJ, Fischman N, Cook P, Wood J, Omasta E. 1970. *Climate, water balance, and climatic change in the northwest Virgin Islands*. Caribbean Research Institute, College of the Virgin Islands.

Bowles JE. 1992. *Engineering Properties of Soils and their Measurement*. McGraw-Hill: New York.

Bren LJ, Leitch CJ. 1985. Hydrologic effects of a stretch of forest road. *Australian Forest Research* **15**(2): 183–194.

Bunte K, MacDonald LH. 1999. *Scale considerations and the detectability of sedimentary cumulative watershed effects*. Technical Bulletin No. 776, National Council for Air and Stream Improvement, Research Triangle Park, North Carolina.

Calversbert RJ. 1970. *Climate of Puerto Rico and the U.S. Virgin Islands*. Climatography of the United States No. 60–52, US Department of Commerce.

Chow VT. 1998. *Handbook of Applied Hydrology*. McGraw-Hill: New York, NY.

Coker RJ, Fahey BD, Payne JJ. 1993. Fine sediment production from truck traffic, Queen Charlotte Forest, Marlborough Sounds, New Zealand. *Journal of Hydrology (New Zealand)* **31**(1): 56–64.

Croke J, Mockler S. 2001. Gully initiation and road-to-stream linkage in a forested catchment, southeastern Australia. *Earth Surface Processes and Landforms* **26**(2): 205–218.

Croke J, Mockler S, Fogarty P, Takken I. 2005. Sediment concentration changes in runoff pathways from a forest road network and the resultant spatial pattern of catchment connectivity. *Geomorphology* **68**(3–4): 257–268.

Dunne T, Leopold L. 1978. *Water in Environmental Planning*. W.H. Freeman: New York, NY.

Dutton AN, Loague K, Wemple BC. 2005. Simulated effects of a forest road on near-surface hydrologic response and slope stability. *Earth Surface Processes and Landforms* **30**: 325–338.

Edwards TK, Glysson GD. 1988. *Field methods for measurement of fluvial sediment*. US Geological Survey Open-File Report 86–531, Washington, DC.

Fahey BD, Coker RJ. 1992. Sediment production from forest roads in Queen Charlotte Forest and potential impact on marine water quality, Marlborough Sounds, New Zealand. *New Zealand Journal of Marine and Freshwater Research* **26**: 187–195.

Flerchinger GN, Watts FJ. 1987. Predicting infiltration parameters for a road sediment model. *Transactions of the ASAE* **30**(6): 1700–1705.

Gardner TA, Côté IM, Gill JA, Grant A, Watkinson AR. 2003. Long-term region-wide declines in Caribbean corals. *Science* **301**: 958–960.

Gee GW, Bauder JW. 1986. Particle-size analysis. In *Methods of Soil Analysis Part 1: Physical and Mineralogical Methods*, Klute A (ed.). American Society of Agronomy: 383–411.

Gray DM. 1960. *Derivation of hydrographs for small watersheds from measurable physical characteristics*. PhD dissertation, Iowa State University of Science and Technology.

Grayson RB, Haydon SR, Jayasuriya MDA, Finlayson BL. 1993. Water quality in mountain ash forests—separating the impacts of roads from those of logging operation. *Journal of Hydrology* **150**: 459–480.

Gresswell S, Heller D, Swanston DN. 1979. *Mass movement response to forest management in the central Oregon Coast Ranges*. USDA Forest Service Resource Bulletin PNW-84, Portland, OR.

Harden CP. 1992. Incorporating roads and footpaths in watershed-scale hydrologic and soil erosion models. *Physical Geography* **13**(4): 368–385.

Helvey JD, Kochenderfer JN. 1990. *Soil density and moisture content on two unused forest roads during first 30 months after construction*. US Forest Service Research Paper NE-629, Radnor, VA.

Henderson FM, Wooding RA. 1964. Overland flow and groundwater flow from a steady rainfall of finite duration. *Journal of Geophysical Research* **69** (8): 1531–1540.

Hubbard DK. 1987. *A general review of sedimentation as it relates to environmental stress in the Virgin Islands Biosphere Reserve and the eastern Caribbean in general*. Biosphere Reserve Report no. 20, Virgin Islands Resource Management Cooperative, St Thomas.

Ice G. 1986. *A study of the effectiveness of sediment traps for the collection of sediment from small plot studies*. NCASI Technical Bulletin 483, New York, NY.

Kahklen KF. 1994. *Surface erosion from a forest road, Polk Inlet, Prince of Wales Island, Alaska*. MS thesis, Oregon State University, Corvallis, OR.

Luce C. 1990. *Analysis of infiltration and overland flow from small plots on forest roads*. MS thesis, University of Washington, Seattle, WA.

Luce CH, Cundy TW. 1992. Modification of the kinematic wave–Phillip infiltration overland flow model. *Water Resources Research* **28**(4): 1179–1186.

Luce CH, Cundy TW. 1994. Parameter identification for a runoff model for forest roads. *Water Resources Research* **30**(4): 1057–1069.

MacDonald LH, Anderson DM, Dietrich WE. 1997. Paradise threatened: land use and erosion on St. John, US Virgin Islands. *Environmental Management* **21**(6): 851–863.

MacDonald LH, Sampson RW, Anderson DM. 2001. Runoff and road erosion at the plot and road segment scales, St. John, US Virgin Islands. *Earth Surface Processes and Landforms* **26**: 251–272.

McCuen RH. 1998. *Hydrologic Analysis and Design*. Prentice Hall: New Jersey.

Megahan WF. 1972. Subsurface flow interception by a logging road in mountains of central Idaho. In *National Symposium on Watersheds in Transition*. American Water Resources Association and Colorado State University: 350–356.

Megahan WF. 1978. Erosion processes on steep granitic road fills in central Idaho. *Soil Science Society of America Journal* **42**(2): 350–357.

Megahan WF, Wilson M, Monsen SB. 2001. Sediment production from granitic cutslopes on forest roads in Idaho, USA. *Earth Surface Processes and Landforms* **26**(2): 153–164.

Montgomery DR. 1994. Road surface drainage, channel initiation, and slope instability. *Water Resources Research* **30**(6): 1925–1932.

Nash JE, Sutcliffe JV. 1970. River flow forecasting through conceptual models, Part 1—a discussion of principles. *Journal of Hydrology* **10**: 282–290.

NRCS. 1998. *Soil survey of the U.S. Virgin Islands*. USDA Report, Natural Resources Conservation Service.

Ramos-Scharrón CE. 2004. *Measuring and predicting erosion and sediment yields on St. John, U.S Virgin Islands*. PhD dissertation, Department of Geosciences, Colorado State University, Fort Collins, CO.

Ramos-Scharrón CE, MacDonald LH. 2003. Measuring and modeling the effects of development on sediment production and delivery, St. John, U.S. Virgin Islands. *Eos, Transactions AGU Fall Meeting Supplement* **84**(46): F755–F756.

Ramos-Scharrón CE, MacDonald LH. 2005. Measurement and prediction of sediment production from unpaved roads, St John, US Virgin Islands. *Earth Surface Processes and Landforms* **30**: 1283–1304.

Ramos-Scharrón CE, MacDonald LH. in press. Development and application of a GIS-based sediment budget model. *Environmental Management*.

Rankin DW. 2002. Geology of St. John, U.S. Virgin Islands. *United States, Geological Survey, Professional Papers* **1631**.

Reid LM. 1981. *Sediment production from gravel-surfaced roads, Clearwater basin, Washington*. Publication FRI-UW-8108, University of Washington Fisheries Research Institute, Seattle, WA.

Reid LM, Dunne T. 1984. Sediment production from forest road surfaces. *Water Resources Research* **20**(11): 1753–1761.

Reid LM, Dunne T. 1996. *Rapid Evaluation of Sediment Budgets*. Catena Verlag: Reiskirchen, Germany.

Rice RM, Tilley FB, Datzman PA. 1979. *A watershed's response to logging and roads: South Fork of Caspar Creek, California, 1967–1976*. USDA, Forest Service, Research Paper PSW-146, Berkeley, CA.

Robichaud PR, Brown RE. 2002. *Silt fences: an economical technique for measuring hillslope soil erosion*. RMRS-GTR-94, US Forest Service, Fort Collins, CO.

Rogers CS. 1998. Coral reefs of the U.S. Virgin Islands. In *Status and Trends of the Nation's Biological Resources*, Vol. I. Haeker P, Doran PD (eds). US Department of the Interior, US Geological Survey: Reston, VA; 322–324.

Sampson RW. 1999. *Road runoff and erosion at the plot and road segment scales on St. John, US Virgin Islands*. MS thesis, Department of Earth Resources, Colorado State University, Fort Collins, CO.

Scott HD. 2000. *Soil Physics—Agricultural and Environmental Applications*. Iowa State University Press: Iowa.

Simons DB, Li RM, Shiao LY. 1977. *Formation of a road sediment model*. Report CER76-77DBS-RML-LYS50, Colorado State University, Fort Collins, CO.

Simons DB, Li RM, Ward TJ, Shiao LY. 1978. *Simple road sediment yield model*. Report CER77-78-DBS-RML-TJW-LYS41, USDA Forest Service, Fort Collins, CO.

Vincent KR. 1979. *Runoff and erosion from a logging road in response to snowmelt and rainfall*. MS thesis, University of California, Berkeley, CA.

Wald AR. 1975. *The impact of truck traffic and road maintenance on suspended-sediment yield from a* 14′ *standard forest road*. MS thesis, University of Washington, Seattle.

Wemple BC, Jones JA, Grant GE. 1996. Channel network extension by logging roads in two basins, western Cascades, Oregon. *Water Resources Bulletin* **32**(6): 1195–1207.

Wemple BC, Swanson FJ, Jones JA. 2001. Forest roads and geomorphic process interactions, Cascade Range, Oregon. *Earth Surface Processes and Landforms* **26**(2): 191–204.

Woodbury RO, Weaver PL. 1987. *The vegetation of St. John and Hassel Island, USVI*. National Park Service, Southeast Region, Research/Resources Management Report SER-83, Atlanta, GA.

Woolhiser DA. 1975. Simulation of unsteady overland flow. In *Unsteady Flow in Open Channels*, Vol. 2, Mahmod K, Yevjevich V (eds). Water Resources Publications: Fort Collins, CO; 485–508.

Ziegler AD, Giambelluca TW. 1997. Importance of rural roads as source areas for runoff in mountainous areas of northern Thailand. *Journal of Hydrology* **196**: 204–229.

Ziegler AD, Sutherland RA, Giambelluca TW. 2000. Partitioning total erosion on unpaved roads into splash and hydraulic components: the roles of interstorm surface preparation and dynamic erodibility. *Water Resources Research* **36**(9): 2787–2791.

Ziegler AD, Giambelluca TW, Sutherland RA. 2001a. Erosion prediction on unpaved mountain roads in northern Thailand: validation of dynamic erodibility modelling using KINEROS2. *Hydrological Processes* **15**: 337–358.

Ziegler AD, Sutherland RA, Giambelluca TW. 2001b. Interstorm surface preparation and sediment detachment by vehicle traffic on unpaved mountain roads. *Earth Surface Processes and Landforms* **26**: 235–250.

DOI: 10.1002/hyp